crystals

MDPI

Communication

Comparison of the Strain Rate Sensitivity in AZ31 and WE43 Magnesium Alloys under Different Loading Conditions

Yudong Lei [1,2], Mei Zhan [2,*], Hai Xin [1,2], Lifeng Ma [3], Yuan Yuan [4], Hongrui Zhang [1,2] and Zebang Zheng [1,2,*]

[1] Research & Development Institute of Northwestern Polytechnical University in Shenzhen, Shenzhen 518057, China
[2] State Key Laboratory of Solidification Processing, Shaanxi Key Laboratory of High-Performance Precision Forming Technology and Equipment, School of Materials Science and Engineering, Northwestern Polytechnical University, Xi'an 710072, China
[3] Heavy Machinery Engineering Research Center, Ministry of Education, Taiyuan University of Science and Technology, Taiyuan 030024, China
[4] National Engineering Research Center for Magnesium Alloys, College of Materials Science and Engineering, Chongqing University, Chongqing 400044, China
* Correspondence: zhanmei@nwpu.edu.cn (M.Z.); zebang.zheng@nwpu.edu.cn (Z.Z.)

Abstract: The initial texture effect of strain rate sensitivity response in magnesium alloys was studied using the quasi in situ electron backscatter diffraction technique. The strain accumulations, under uniaxial loading of both tensile and compression along the rolling direction, showed strain rate dependency. For the AZ31 magnesium sheets with strong basal texture (max intensity to 11.2), twinning first occurs at the onset of plastic deformation, resulting in macroscopic strain rate insensitivity. With further loading, the strain rate sensitivity significantly increases (with the strain rate sensitivity coefficient *m* increased from 0.0025 to 0.012), arising from the initiation of slip. For the WE43 alloy sheets with weak basal texture (max intensity to 2.6), the overall deformation is sensitive to strain rate under both tensile and compression. The twinning growth rate and twinned volume fraction have been used to identify whether the process is twin-dominated or slip-dominated during the plastic deformation of a magnesium alloy.

Keywords: magnesium alloy; strain rate sensitivity; twinning; slip

check for updates

Citation: Lei, Y.; Zhan, M.; Xin, H.; Ma, L.; Yuan, Y.; Zhang, H.; Zheng, Z. Comparison of the Strain Rate Sensitivity in AZ31 and WE43 Magnesium Alloys under Different Loading Conditions. *Crystals* **2023**, *13*, 554. https://doi.org/10.3390/cryst13040554

Academic Editor: Bolv Xiao

Received: 6 March 2023
Revised: 21 March 2023
Accepted: 22 March 2023
Published: 23 March 2023

Copyright: © 2023 by the authors. Licensee MDPI, Basel, Switzerland. This article is an open access article distributed under the terms and conditions of the Creative Commons Attribution (CC BY) license (https://creativecommons.org/licenses/by/4.0/).

1. Introduction

Magnesium alloys have gained increasing attention as potential materials to reduce the weight of vehicles in the past two decades. Their mechanical properties, such as strength, anisotropy, ductility, etc., have been extensively studied. Specifically, rate-dependent plasticity has a great influence on the deformation behavior of magnesium alloys [1], while the magnesium components of automobiles or aerospace are often manufactured and serviced under different strain rates [2,3]. Therefore, it is important to understand the deformation characteristics of magnesium alloys and their influencing mechanism with respect to strain rates.

It is well accepted that strain rate hardening may influence the formability of metals. Several studies have examined the strain rate sensitivities (SRSs) of magnesium alloys. The rate-sensitive behaviors corresponding to their complex deformation mechanism have been revealed as a result [4,5]. One of the critical findings is that the SRS of magnesium alloys exhibits obvious dependency on strain paths since only slip contributes to the rate-dependence of the material. For example, Kurukuri [6,7] studied the strain rate sensitivity through tensile and compressive tests of AZ31B sheets at room temperature over the strain rate range from 0.001 to 1000 s^{-1} and found that magnesium alloy sheets exhibit strong SRS during slip-dominated deformation processes, e.g., in-plane tension, while showing to be nearly strain rate insensitive during twin-dominated deformation processes, e.g., in-plane

compression [8–10]. When the c-axis of the hexagonal close-packed (HCP) structure is subjected to an extension, tension twins may be easily generated (i.e., a twin-dominated deformation). In contrast, when contraction is applied nearly parallel to the c-axis, both ⟨a⟩-basal slip and compression twins are activated (i.e., a slip-dominated deformation since the resistance of basal slip is lower) [11].

In addition, a strong texture can be formed for the magnesium alloy sheets during the rolling process, which can also significantly affect the mechanical responses of the material. The stronger the texture intensity, the greater the variation in the rate-dependent behavior of the material under various deformed conditions [12]. Therefore, the impact of initial texture on the strain rate sensitivity of magnesium alloys should be considered in addition to the external loading conditions.

Although many studies have been conducted investigating the SRS of magnesium alloys, the majority mainly focused on the onset of yield or a certain strain of the deformation. However, the SRS may vary during the deformation process, especially for the material that experiences the competition between slip and twinning, as in magnesium alloys. In order to further understand the variation of SRS of magnesium alloys, it is necessary to study the rate-dependent behavior during the entire deformation process.

In the present work, two magnesium alloys, AZ31 and WE43, were chosen as the investigation object. These two alloys are commonly used to manufacture lightweight components in the industry, and they have distinct initial textures [13,14]. The strain rate sensitivity of different textures can thus be studied and compared by employing microscopic characterizations and mechanical tests in tension and compression. The microstructure evolution during the whole deformation process is monitored using the quasi in situ electron backscatter diffraction (EBSD) technique, aiming to understand the competition between slip and twinning at different strain levels and how it affects the strain rate sensitivity of magnesium alloys with different initial textures.

2. Experimental Procedures

- Material and characterization

The investigated AZ31 alloy and WE43 alloy with a nominal composition of Mg-3Al-1Zn (wt%) and Mg-rare-earth alloys class, respectively, were manufactured by the rolling technique. The thickness of these two kinds of magnesium alloy sheets was identical, i.e., 8 mm. Microstructure and crystallographic orientation observations were carried out using a ZEISS Sigma 300 field emission scanning electron microscope with Oxford Instrument Nordlys Nano EBSD detector. The observation plane contained the rolling direction (RD) and the transverse direction (TD). Specimens for EBSD observations were ground and mechanically polished until 4000 grit silicon carbide papers, followed by electrochemical polishing in AC-II for 70 s at 0.05 A/20 V.

- Mechanical property testing

Flat dog-bone tension specimens, with gauge dimensions of $18 \times 4 \times 2.5$ mm^3 (length $\times$ width $\times$ thickness) and cuboid compressive samples with dimensions of $8 \times 8 \times 5$ mm^3, were fabricated using an electric spark machine from the hot-rolled sheets in Figure 1a. The length and width of the samples paralleled RD and TD, respectively. Using an Instron-8801 testing machine, room temperature uniaxial tension and compression tests were carried out along RD with 4 different strain rates ranging from 1×10^{-4} s^{-1} to 1×10^{-1} s^{-1}. For the sake of repeatability and accuracy, at least three repeat tests were performed for each condition. The strain during deformation was measured and recorded using a non-contact laser extensometer mounted on an Instron-8801 testing machine. The engineering strain and stress were used in the present study unless otherwise stated. For the purpose of examining the variation of SRS during tensile or compression with increasingly imposed strains, the SRS factor was calculated by using the offset strain method with elastic modulus as the slope. The conventional yield stresses were determined using the 0.2% offset strain method.

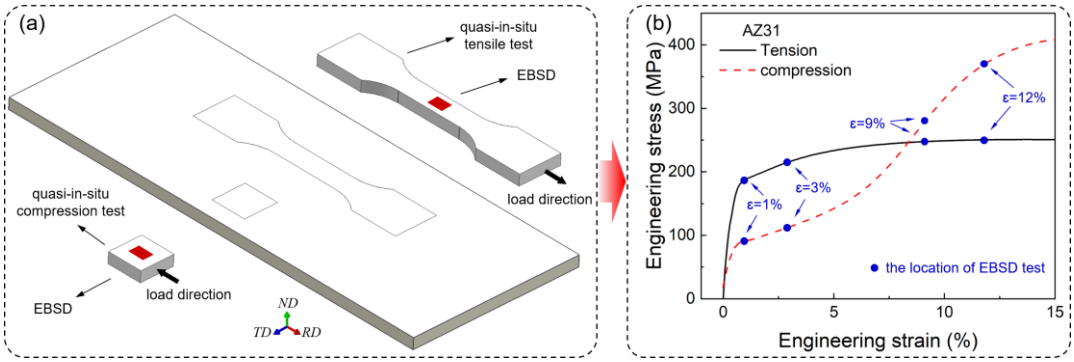


Figure 1. (**a**) The schematic diagram of the sample fabrication and (**b**) the quasi in situ performance curves of the as-rolled AZ31 specimens. (**a**) Tensile and compression samples of AZ31 and WE43 were fabricated from the as-rolled plate, followed by a quasi in situ EBSD test on the ND surface of the samples. (**b**) Quasi in situ EBSD tests were conducted at strain levels of 1%, 3%, 9%, and 12%, both tension and compression.

In order to understand the microstructural evolution during the deformation, the tensile and compressive experiments were interrupted at the designed strain levels, and EBSD characterization was conducted in the identical areas within the gauge section of the specimen (the locations with blue marked are shown in Figure 1b). Note that no further treatment was made on the deformed surface during the interrupted loading to avoid artificial effects. The selected area (the red marked area is shown in Figure 1a) for characterization contains approximately 500–1000 grains. The step size for undeformed and deformed samples was chosen to be 1.5 μm and 0.8 μm, respectively, to ensure that the average EBSD indexing ratio was beyond 85% for all the tested samples. An in-house MATLAB code, which was developed based on the open-source toolbox MTEX, was used to analyze the raw EBSD orientation data [15].

3. Results and Discussion

3.1. Microstructures before Loading

Figure 2 demonstrates the initial microstructure, including the grain morphology and crystal orientation distributions, for the AZ31 and WE43 alloys before uniaxial loading tests. The inverse pole figure (IPF) maps in Figure 2a,c demonstrate that these two alloys possess uniform and equiaxed microstructures without any twins. The average grain sizes were measured as 15 μm and 10 μm for the AZ31 and WE43 sheets, respectively. Both grain sizes are higher than the value where the size effect is noticeable, e.g., 2 μm [16]. Therefore, the differences caused by the initial grain size of these two alloys are negligible in the present study. Furthermore, the initial textures of these two alloys are dramatically different, as shown in Figure 2b,d. The AZ31 alloy exhibited a strong basal texture with the c-axis of most grains parallel to ND. In comparison, the WE43 alloy possesses a weakened basal texture due to the presence of rare earth elements. Therefore, the anisotropy of mechanical characteristics under uniaxial tension and compression is expected to differ due to the distinct texture. In this study, the loading direction for both compression and tension in the two alloys is parallel to RD, as shown in Figure 2.

3.2. Mechanical Behavior

Due to the different textures of these two magnesium alloys, their mechanical responses are also significantly different from each other. The data in Figure 3 show the engineering stress versus engineering strain from uniaxial tensile and compressive tests under different strain rates along the RD. From Figure 3a,b, engineering stress clearly increases with the strain rate, i.e., both alloys show obviously positive strain rate sensitivity in tension. This mechanical behavior is mainly attributed to the strain rate dependency of the critical resolve shear stress (CRSS) of non−basal slip systems [17]. Moreover, the

hardening rate is similar between the considered materials, while the yield strength of the WE43 alloy is slightly higher than that of the AZ31 alloy under the same strain rate.

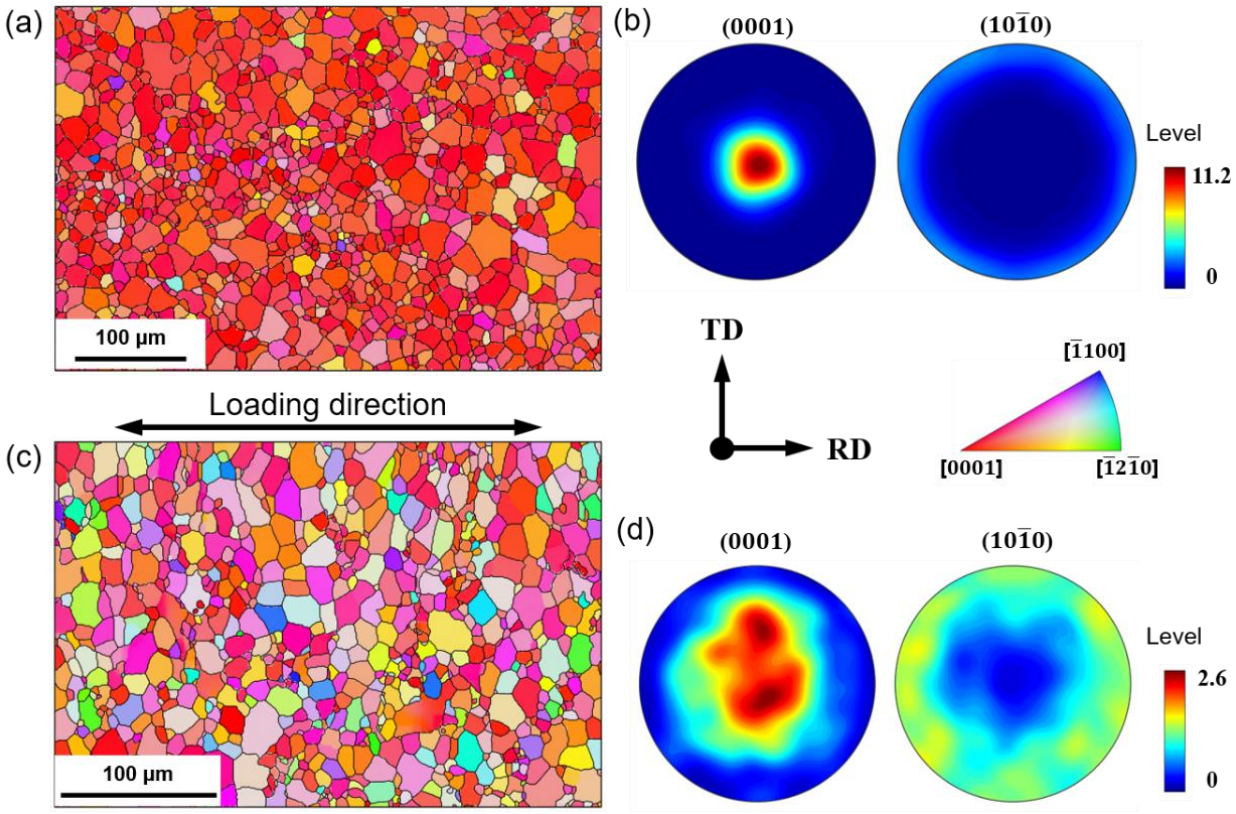


Figure 2. The inverse pole figure maps and pole figures of (**a**,**b**) the AZ31 alloy and (**c**,**d**) the WE43 alloy before deformation. The IPFs map shows that both (**a**) AZ31 and (**c**) WE43 alloys possessed uniform and equiaxed microstructures without any twins. (**b**) The PF map of the AZ31 alloy demonstrated that it has a strong (0001) basal texture with the max intensity of 11.2. (**d**) The PF map of the WE43 alloy showed more weakened basal texture compared with the AZ31 alloy, with the max intensity of 2.6.

In addition, the engineering stress–strain curves of the AZ31 and WE43 alloys under compression with different strain rates are provided in Figure 3c,d, which is obviously different compared to tension. On the one hand, for the WE43 alloy, the development of the flow stress with the strain is similar to the tensile tests. The hardening rate barely changes during the loading, although the value is higher than that of tension. The yield strength under compression is also enhanced by the strain rate. On the other hand, for the AZ31 alloy, at the onset of yield, the material experiences almost strain-rate-independent deformation followed by the hardening rate increasing dramatically and then gradually reducing. After~8% engineering strain, the AZ31 alloy starts to display a positive strain rate sensitivity. The variation of the rate dependence with strain, which is consistent with trends reported by earlier studies [4], is due to the activation of multiple plastic deformation mechanisms. The fraction of the contribution from slip and twinning determines the macroscopic strain rate sensitivity.

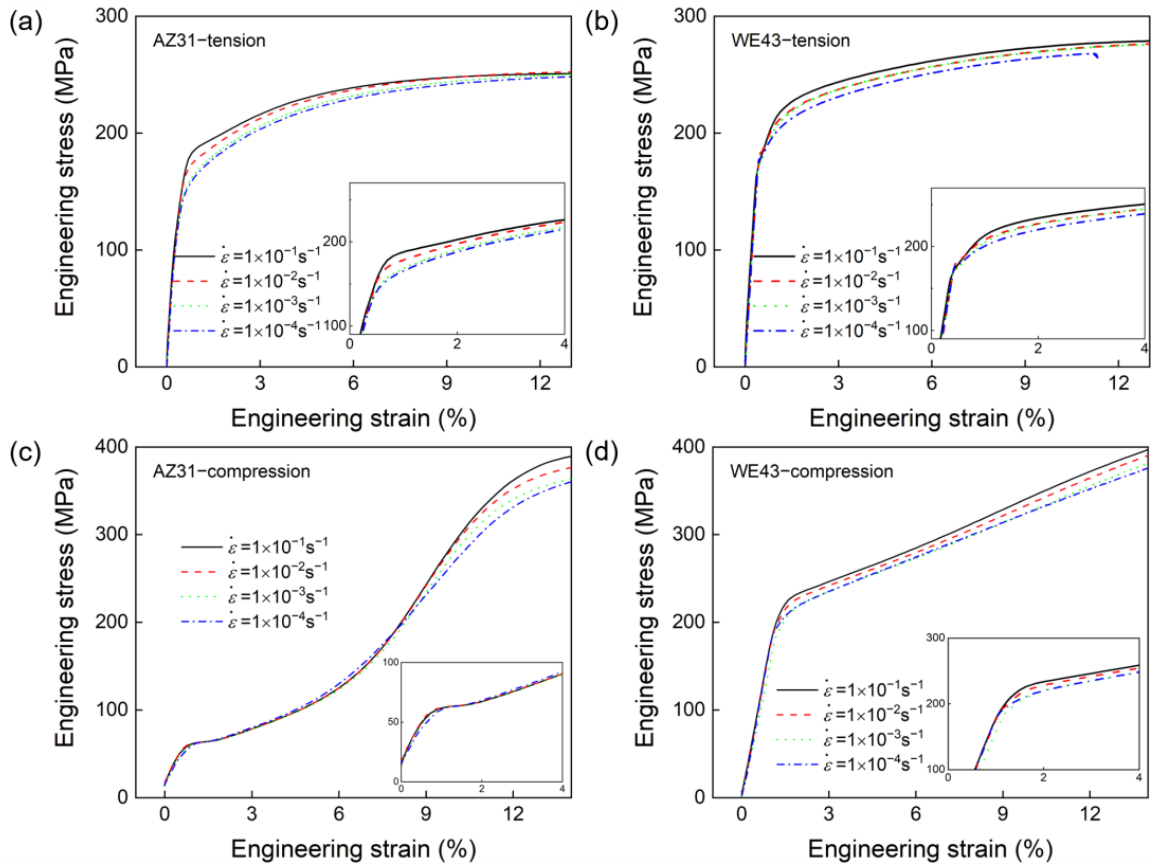


Figure 3. Engineering stress−strain curves of the AZ31 and WE43 alloy samples in RD: (**a**,**b**) tensile; (**c**,**d**) compression under different strain rates. Both (**a**) AZ31 and (**b**) WE43 alloy samples showed obviously positive strain rate sensitivity in tension. This mechanical behavior was ascribed to the strain rate dependency of non-basal slip systems. (**c**) The mechanical behavior of the AZ31 alloy showed strain rate independence in the early deformation stage under compression. Then, it exhibited a positive SRS as the engineering strain increased to 8%. This can be mainly attributed to the influence of the interplay between twinning and slip. (**d**) The evolution of flow stress with the strain was similar to that observed in the tensile test of (**b**) the WE43 alloy.

4. Strain Rate Sensitivity Evolutions under Different Loading Conditions

Comparing the tensile and compressive responses for the same material, the AZ31 alloy clearly shows tension–compression asymmetry. The S-shaped stress–strain curve is observed under compression, which does not occur under tension, while for the WE43 alloy, where the basal texture is weaker, the tension and compression stress–strain curves have a similar trend. The differences in tension–compression asymmetry are raised from the crystal orientation distributions, which lead to the activation of slip and twinning at different levels. Since the contribution to the rate-dependent plasticity from slip and twinning are different, the resultant SRS is also different. More importantly, the SRS component also varies with the development of strain.

For further exploration, the 0.2% yield strength of these two alloys as a function of strain rate is summarized in Figure 4. As shown in Figure 4a, the yield strength for AZ31 under compression is only about half of the value under tension. This behavior can mainly be attributed to the generation of tension twins at the early stage of the AZ31 alloy under compression. The required stress to drive tension twin nucleation is lower for the initiation of slip for the given strong texture, where resolved shear stress for basal slip is near zero.

To quantitatively evaluate the strain rate sensitivity, the strain rate sensitivity coefficient m is calculated according to the method of constant strain rate given by

$$m = dln\sigma_{0.2}/dln\dot{\varepsilon} \quad (1)$$

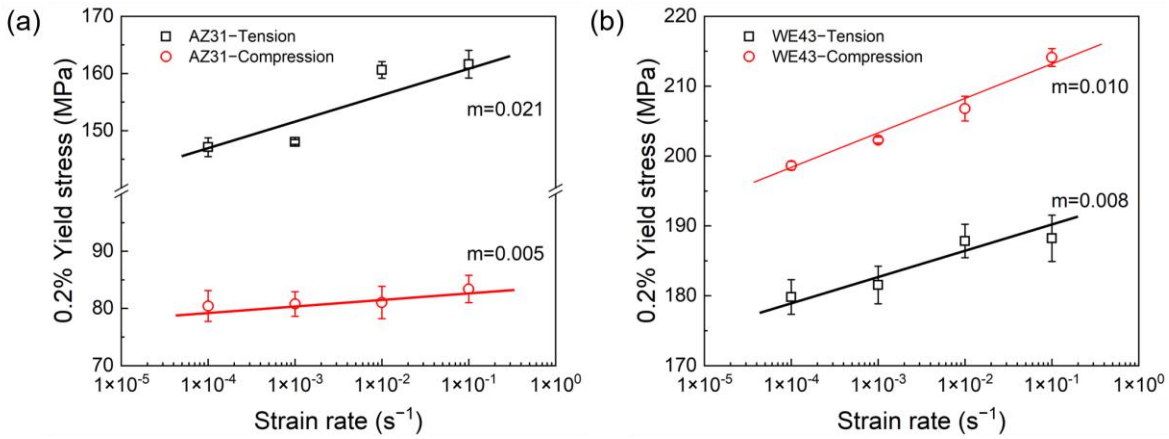


Figure 4. The yield stress (the 0.2% offset) under different strain rates for the (**a**) AZ31 and (**b**) WE43 alloy under uniaxial tension and compression: (**a**) The SRS factor of the AZ31 alloy under tension was 0.021 on the yield stress but only 0.005 under compression deformation. It exhibited obvious tension–compression asymmetry, which is attributed to the presence of tension twinning during the early stage of deformation. (**b**) The SRS factor of the WE43 alloy under the same conditions were 0.008 and 0.010 for both tension and compression, respectively, revealing that the SRS was hardly influenced by the loading direction.

Through repeated tests, the tensile and compression m values of the AZ31 alloy are obtained as 0.021 and 0.005, respectively. A positive strain rate sensitivity is dominated by dislocation slip at the onset of yield during tensile tests, while the compression shows strain rate insensitivity, which is dominated by twinning deformation. There is a significant strain rate sensitivity asymmetry for the AZ31 alloy. The m values of the WE43 alloy under the same conditions are found to be 0.008 and 0.010 for tension and compression respectively, as shown in Figure 4b, indicating that the strain rate sensitivity for the alloy is barely affected by the loading direction. In light of this, the plastic deformation at the onset of yield for the WE43 alloy is predominated by slip for both loading directions, owing to the weaker basal texture.

The difference in the strain rate sensitivity of magnesium alloys mainly results from variations in the dominant deformation mechanism of slip and twinning. Numerous review studies have explored this phenomenon across different alloy materials [11,18–20]. However, the materials studied in this paper exhibits a distinctive difference in strain rate sensitivity, primarily due to differences in initial texture and loading conditions.

In addition to the difference in the strain rate sensitivity at the onset of yield, another important observation from Figure 4 is that the SRS changes as a function of the imposed strain throughout the deformation process. For quantitatively evaluating the rate dependent of magnesium alloys for the entire deformation in terms of the imposed strain, the m value calculated through Equation (1) is shown in Figure 5. There is a significant change in m under different loading conditions. As shown in Figure 5a, the m value for the AZ31 alloys under tension decreased from 0.22 to 0.005 as the strain increased. This indicates that the contribution from dislocation gliding reduces at higher strains. However, for compression, the m value shows approximately 0.0025 at the early stage of deformation (e.g., engineering strain < 4%). The low strain rate sensitivity with m value approaches zero at low strain resulting from the formation of extension twins. Due to the apparent {0001} basal texture in Figure 2a, twinning is more easily activated than slip when the compression direction is perpendicular to the <c>-axis of the hexagon. Moreover, as the strain increased

up to 12%, the *m* value gradually grew to about 0.012, as shown in Figure 5a. This suggests that the deformation mechanism transforms from twin-dominated to slip-dominated deformation. At higher imposed strains, due to the changing of local stress states resulting from twin formation, more slip systems are activated, and the dislocation movement becomes easier, which leads to the increase of strain rate sensitivity. Macroscopically, the tension and compression responses of the AZ31 alloy sheets exhibited obvious strain rate sensitivity asymmetry.

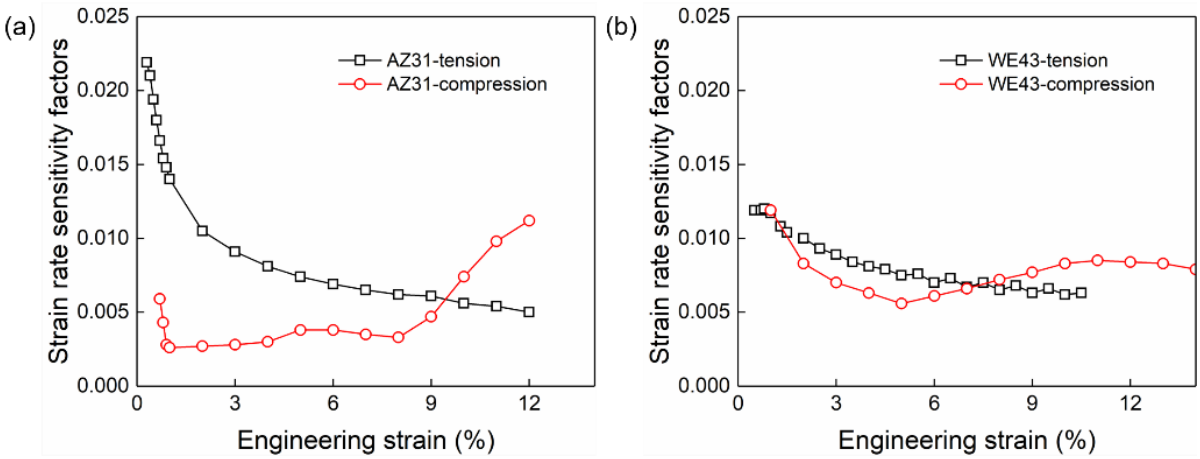


Figure 5. Strain rate sensitivity factors for the (**a**) AZ31 and (**b**) WE43 alloys under uniaxial tension and compression. (**a**) The SRS factor, *m*, decreased dramatically for AZ31 tension as the strain increased, but for compression, the low SRS with *m* value approached zero at low strain. Then, the sample exhibited strain rate dependence at higher imposed strains, which is caused by more slip systems activated and the dislocation movement. (**b**) The trend of the SRS factor of the WE43 alloy was similar to the AZ31 alloy, dropping from 0.012 to 0.006 under tension. This showed that the materials proved a positive SRS due to slip-dominated deformation. For the compression, the *m* value decreased firstly at the low strain regime and then arose slowly at the high strain regime, which is caused by slip deformation and twin behavior occurring simultaneously and affecting each other.

For the WE43 alloy in Figure 5b, it is interesting to note that the *m* value has dropped from 0.012 to 0.006 under tension. This indicates that the material exhibits a positive strain rate sensitivity due to the slip-dominated deformation process. With further strain, the interactions between dislocations become stronger and make their movement more difficult. As a result, the hardening effect overrides the rate-dependent plasticity. As for the compression, the *m* value decreases from 0.012 to 0.005 at the low strain regime (strain < 5%) and then ascends slightly to 0.009 at the high strain regime. It reveals that slip deformation and twin behavior take place simultaneously and impact each other. The basal slip is gradually activated as the strain increases, accompanied by a small amount of twinning due to the WE43 alloy sheets with weakened basal texture. With further straining, the competition between slip and twinning becomes more significant, which leads to the variation of SRS.

5. Overall Texture Evolutions in AZ31 and WE43 Alloys

In order to understand the changes in strain rate sensitivity of these two alloys, a detailed microstructural evolution investigation, with particular attention focused on texture, was performed during the tension and compression tests by tracking the different strain levels on the sample surface. The EBSD results show the as-rolled AZ31 alloys at strains of 1%, 3%, 9%, and 12% in Figure 6, respectively, during the quasi in situ tensile test. The IPF diagram and special grain boundary diagram are used to demonstrate the microstructure evolution of the specimen during the tensile process.

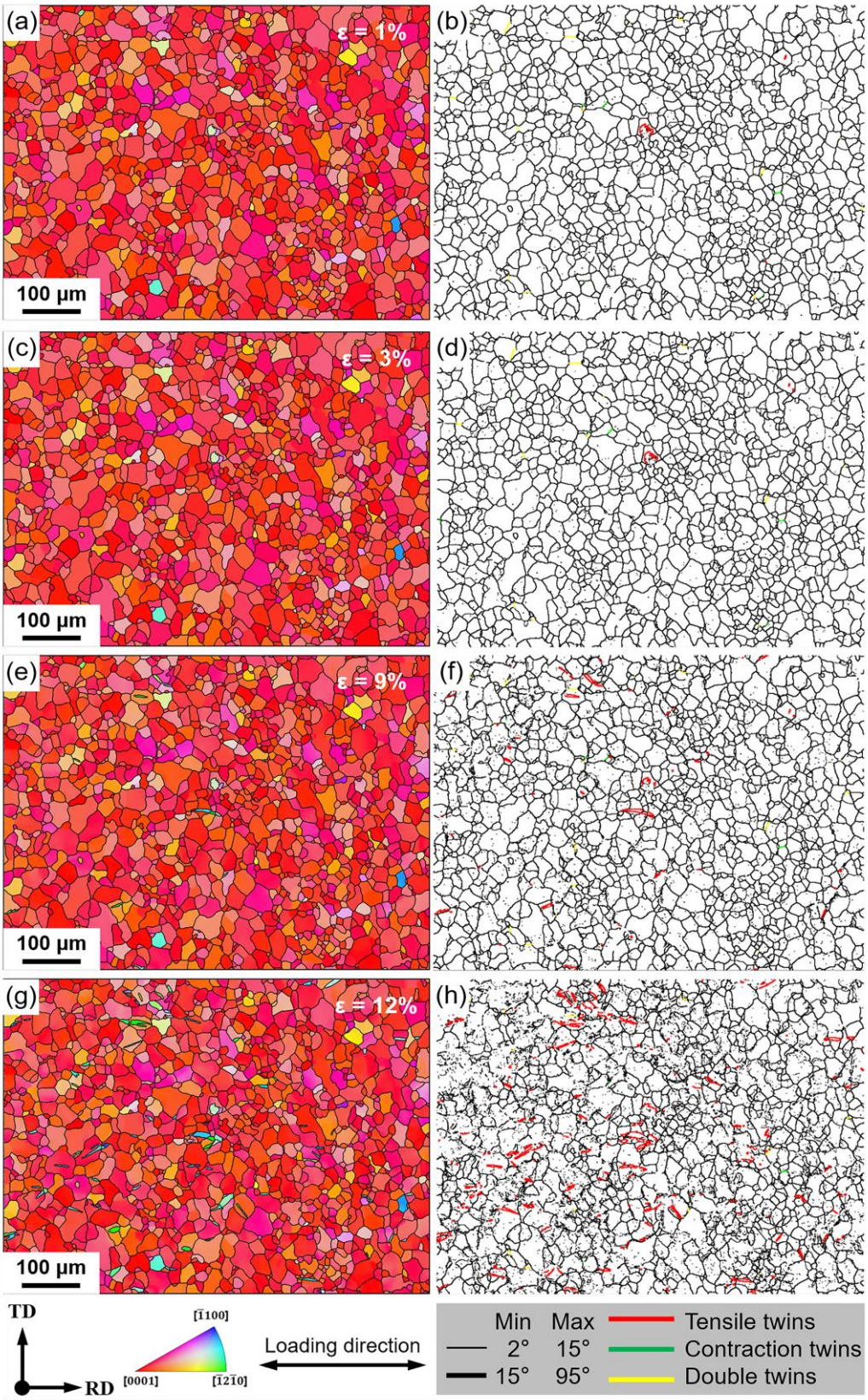


Figure 6. Quasi in situ EBSD evolution results of rolled AZ31 alloys in the tensile direction: (**a**,**c**,**e**,**g**) the IPF maps and (**b**,**d**,**f**,**h**) special grain boundary diagrams at different stages. (**a**–**d**) From the IPF maps and special grain boundary diagrams, it is evident that none of the twinning presents at a low strain level (strain < 3%). (**e**–**h**) The small portion of twinning emerged inside some grains when the strain surpasses 9%.

Figure 7 illustrates the evolution of the (0001) pole figure for both magnesium alloys during the loading. The (0001) pole figures are shown at the strains of 1%, 3%, 9%, and 12%, according to the key variation points in the strain rate sensitivity factors of both magnesium alloys.

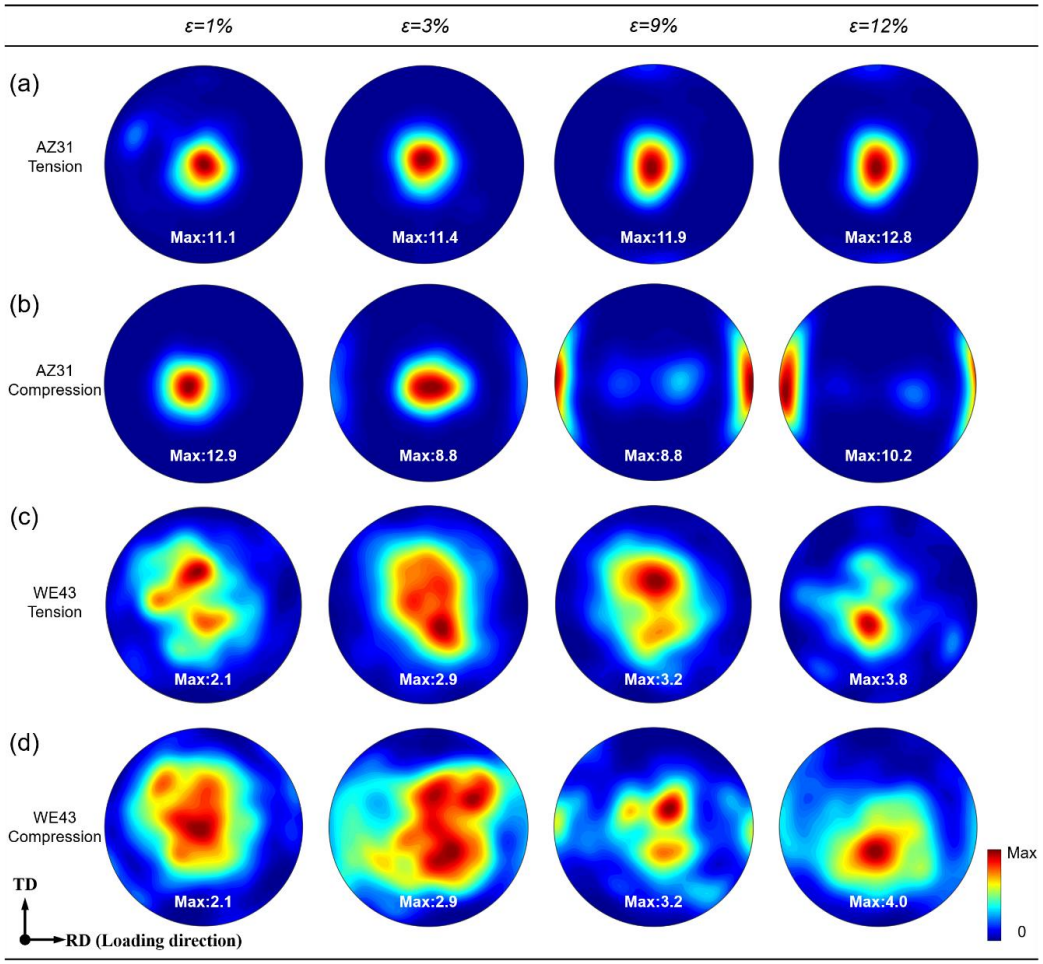


Figure 7. The evolutions of (0001) pole figures in the (**a**,**b**) AZ31 and (**c**,**d**) WE43 alloy under different loading conditions. (**a**) The texture type of the AZ31 alloy remained nearly unvaried during tension. (**b**) For the compression, the intensity of basal texture weakened as the strain increased from 1% to 3%. It was attributed to the presence of tension twinning at a low strain regime, leading to an 86° rotation of the <11–20> axis. The <c> axis of most grains is reoriented to be parallel to the loading direction at a higher strain regime (strain > 9%). (**c**,**d**) The evolution of texture type of the WE43 alloy for both tension and compression were not changed, and the (0001) pole figure is more concentrated as the strain increases.

For tension in the AZ31 alloy, it can be clearly seen that the texture type remains almost unchanged during the whole process, as shown in Figure 7a. The <c> axis of most grains in the sample is aligned with the ND. The orientation of most grains remained unchanged since the ⟨c + a⟩ pyramidal slip and contraction twin were activated when the <c> axis was compressed. However, these systems are not expected to be activated at room temperature since the corresponding CRSS is higher than 50 MPa, [21–23]. Therefore, the ⟨a⟩ basal slip system was activated, and the deformation was governed by slip. As shown in Figure 7a, the texture intensity was slightly increased when the strain reached 12%. This change corresponds to the m value decreasing in Figure 5a, where the interactions between dislocations hinder their movements and result in a stronger hardening.

For compression in the AZ31 alloy, it is noted that the trend of texture evolution is different from tension. The basal texture becomes weaker under compression at the strain of 3%. Twinning took place at the first stage of the deformation, leading to an 86°

rotation of the <11–20> axis, which brings it into alignment with the compression axis. The compression strength is low due to the low activating stress of the tension twin being only 3.5 MPa. This is the fundamental explanation for the tension–compression asymmetry of the AZ31 alloy. With the further increase of strain (up to 9%), the <c> axis of most grains was reoriented to be parallel to RD. Combined with Figure 5a, it can be concluded that the twinning is rate-independent. This twinning behavior is followed by a strong strain-hardening at larger strains owing to the activation of non-basal slip [4,8,17]. The plastic deformation mechanism thus transforms from twin-dominated to slip-dominated, leading to the variation of *m* value in Figure 5a.

On the contrary, the texture of WE43 alloy was not changed significantly under both tension and compression, as shown in Figure 7c,d. The intensity of the (0001) pole figures under tensile developed from 2.1 to 3.8 as the strain increased to 12%. Simultaneously, it was observed that the (0001) pole figure is more concentrated at large strains. Dislocations piling up at grain boundaries twist the lattice, and this phenomenon becomes stronger with strain increases. According to the strain rate sensitivity factors in Figure 5a,b, the *m* value for the WE43 alloy under tensile was similar to the AZ31 alloy with the strain rises, leading to a similar deformation mechanism.

For compression in the WE43 alloy, the type and intensity of texture were similar to its tension responses. As shown in Figure 5b, the strain rate sensitivity factor decreased at the early stage of the deformation, indicating that twinning is simultaneously generated. The orientation of grains was not considerably changed under compression deformation, revealing that partial twinning is produced. In order to further investigate the effect of twins on texture evolution and strain rate sensitivity, twin volume fraction (TVF) analyses at different strain regimes are required.

Therefore, the mechanical performance in Figure 3 and the texture evolution in Figure 7 highlight a significant difference in tension–compression asymmetry between the AZ31 and WE43 alloys. When forming components using the same loading conditions, the evolution of the texture type of magnesium alloy can lead to-defects forming and adversely affect the material's formability.

6. Twinning Growth Rate and Twinned Volume Fraction

The evolution of the TVF in the AZ31 and WE43 alloys was quantitatively evaluated under tension and compression, as shown in Figure 8. For the AZ31 alloy in Figure 8a,b, the evolution of TVF shows significant differences under tension and compression. As the strain increases, the maximum value of the TVF increases slowly by approximately 6.5%, indicating that the tension deformation of the AZ31 alloy along RD was still dominated by slips. Furthermore, as shown in Figure 7a, when the strain is between 1 and 3%, the texture type does not change considerably, which further confirms that the deformation is not dominated by twinning. Meanwhile, due to the slip-dominated deformation, dislocations may pile up at grain boundaries during the tension process. The microstructure of the AZ31 alloy has an uneven local stress distribution. Moreover, the twinning behavior may occur such that the local stress state is no longer uniaxial tension which explains the TVF increase. As a consequence, twin-dominated deformation processes were found to be strain rate insensitive. It also contributes to the reduction of strain rate sensitivity in later deformation.

When the AZ31 alloy was subjected to compression, the TVF rapidly increased when the engineering strain was below 3%. It is attributed to the enormous number of twin nucleation at the initial plastic deformation stage. At this stage, the <c> axis of most grains was still parallel to the ND, which is consistent with the pole figure in Figure 7b. It demonstrated that the twin-dominated deformation processes exhibited significant strain rate insensitivity at the early deformation stage. Furthermore, the TVF kept increasing with further strains. The existing twin grains absorbed the matrix grains through the transfer of twin boundaries at this stage, which is primarily the twin growth process. It is worth noting that the growth of twin grains which mainly generated tension twin, shifted from the 'soft' orientation to the 'hard' orientation. Moreover, slip systems were activated to

coordinate the deformation since the tensile twinning can only accommodate a limited strain, resulting in improving the strain rate sensitivity factor (highlighted by the solid black arrow in Figure 8b. The strain rate sensitivity factor fluctuates between 5% and 8%. It is considered that the competition between slip-dominated and twin-dominated has emerged. The increasing trend of the twinned volume fraction decelerated when the engineering strain approached 8%. The texture of the AZ31 alloy transformed (0001)||ND to (0001)||RD as in Figure 7b. The increasing tendency of TVF tends to stay stable as the amount of deformation increases. It is consistent with the pole figure for the strain of 12% in Figure 7b, where the texture type has not been changed. The contributions of twinning behavior to the sample deformation gradually drop, and the non-basal plane slip system is activated to coordinate plastic deformation for the AZ31 alloy. As a consequence, the twin-dominated deformation is considered to evolve into the slip-dominated deformation at the later stage of deformation, leading the strain rate sensitivity factor to gradually increase, which is consistent with the observation in Figure 8b (indicated by the solid red arrow).

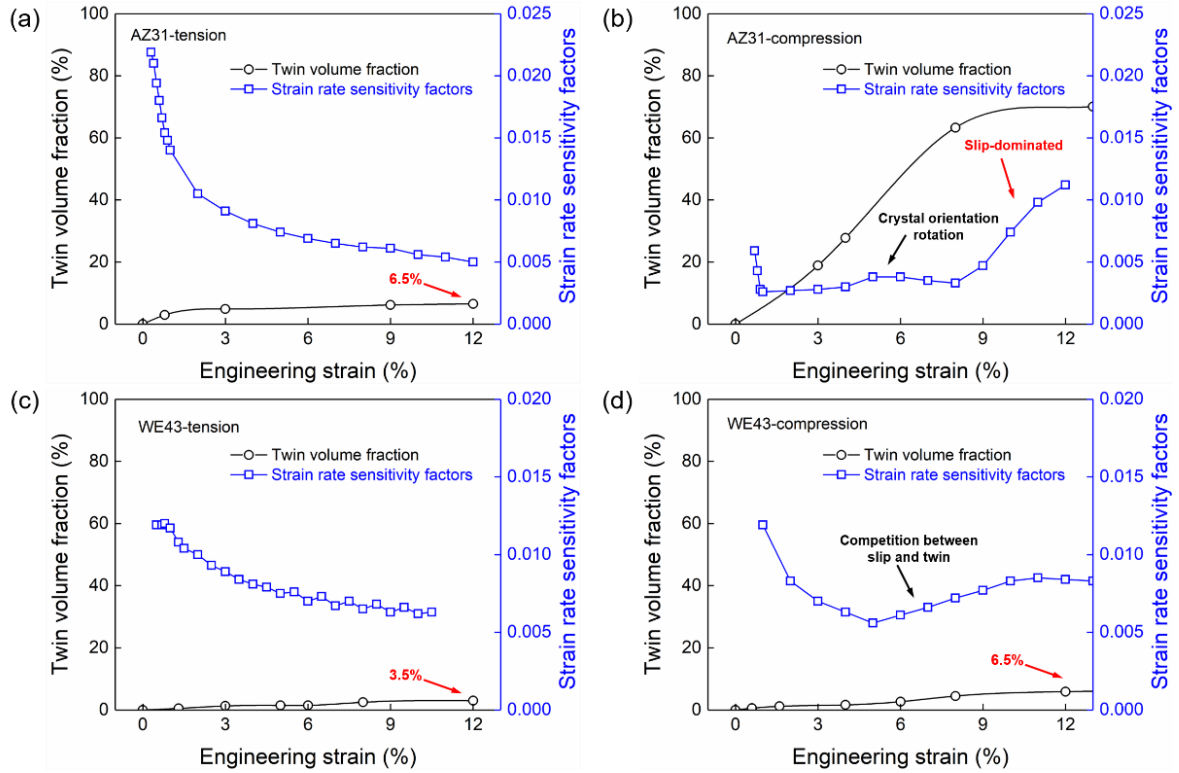


Figure 8. The evolution of twin volume fraction and strain rate sensitivity factors of (**a**,**b**) AZ31 and (**c**,**d**) WE43 alloys during uniaxial tension and compression. (**a**) The maximum value of the TVF during AZ31 tension increased slightly by 6.5%. It indicated that this process was dominated by slip deformation. (**b**) For the AZ31 compression, the TVF rapidly ascended at the strain level of 1~9%, which was attributed to the abundance of twin nucleation and growth. It indicated that the SRS factors appeared as a negative SRS at this deformation stage. As the strain increased to 12%, the TVF of AZ31 tend to stabilize. The influence of twinning behavior on sample deformation gradually decreased, and a non-basal plane slip system was activated to accommodate deformation, leading to the increase of SRS. (**c**) The trend of TVF of WE43 alloy was similar to AZ31 during tension deformation. (**d**) The SRS factor of WE43 was affected by the presence of a small amount of twinning during compression, and the fluctuation of SRS was mainly attributed to competition between slip-twin deformation processes.

The evolution of the TVF of the WE43 alloy sample is not particularly different under tension and compression deformation. For tension, the TVF increases slightly by just 3.5% with further loading up to strain 12%. It demonstrated that the deformation mechanism of the WE43 alloy during tension was slip-dominated, which is consistent with the change of the AZ31 alloy in Figure 8a. The SRS factor decreases gradually during tension. As shown in Figure 7c, the basal texture gradually concentrated from a discrete form to a certain point. Therefore, the slight variation in texture is considered to be generated by two aspects. The material lattice rotates as the increasing deformation and a small amount of inside twinning behavior induce the texture fluctuation.

For compression, the TVF of the WE43 alloy differs significantly from that of the AZ31 alloy. Most grains do not nucleate tension twin under compression, according to the weak initial texture of the WE43 alloy. The addition of rare earth elements inhibits twinning behavior while facilitating non-basal plane slip activation [24]. It indicated that the deformation mechanism of the WE43 alloy during compression was slip-dominated. The TVF did not significantly increase as the amount of deformation developed. As shown in Figure 8d, it only reached 6.5% when the applied strain was 12%. It was noted that the SRS factor dropped from 0.012 to 0.006 at strain to 6%. With the strain imposed, the strain rate sensitivity factor increases again up to 0.009. The emergence of twinning behavior had an influence on the SRS at this deformation stage. The variation of the SRS was thus attributed to competition between slip-twin deformation processes.

7. Conclusions

The effect of initial texture on the strain rate sensitivity and tension–compression asymmetry in the AZ31 and WE43 alloys was investigated using the quasi in situ EBSD technique. Under the tensile deformation along RD, the AZ31 alloy with a strong basal texture was found to be sensitive to strain rate, while in compression, it is insensitive. On the other hand, the WE43 alloy with a weak texture is susceptible to strain rate in both tension and compression. The tensile SRS factor of AZ31 steadily reduced as the strain increased, which is attributed to slip-dominated deformation. For compression, the SRS factor of AZ31 first declined and then increased. The main reason for this phenomenon was the evolution of twin-dominated deformation into slip-dominated deformation. The evolution of the SRS of the WE43 alloy was similar to the AZ31 alloy under tension and compression deformation. Fewer twins were developed by the WE43 alloy with a weak texture, which slightly affected the SRS factor. It was further demonstrated that the twinning behavior had an influence on the SRS in both tension and compression. This study provides insights into the deformation mechanisms of the initial texture of different types of magnesium alloys under different strain rates and loading conditions, which are valuable for designing and optimizing magnesium alloys to manufacture lightweight components for various industrial applications.

Author Contributions: Conceptualization, methodology, investigation and formal analysis, Y.L.; investigation and visualization, H.X.; writing—original draft preparation, Y.L.; writing—review and editing, Z.Z.; project administration, M.Z.; funding acquisition, M.Z. and Z.Z.; investigation, L.M.; investigation, Y.Y.; investigation, H.Z. All authors have read and agreed to the published version of the manuscript.

Funding: This research was funded by the NSFC-Shanxi Coal Based Low Carbon Joint Fund, grant number: U1910213, the National Science and Technology Major Project, grant number: J2019-VII-0014-0154 and Shenzhen Science and Technology Program, grant number: JCYJ20220530161814031, JCYJ20190806151614583.

Data Availability Statement: Not applicable.

Conflicts of Interest: The authors declare no conflict of interest.

References

1. Wang, H.; Wu, P.; Kurukuri, S.; Worswick, M.J.; Peng, Y.; Tang, D.; Li, D. Strain Rate Sensitivities of Deformation Mechanisms in Magnesium Alloys. *Int. J. Plast.* **2018**, *107*, 207–222. [CrossRef]
2. Muniandy, T.; Abdullah, N. Carbon Nanotubes (CNTs)-Reinforced Magnesium-Based Matrix Composites: A Comprehensive Review. *Materials* **2022**, *13*, 1–15. [CrossRef]
3. Abazari, S.; Shamsipur, A.; Bakhsheshi-Rad, H.R.; Ramakrishna, S.; Berto, F. Graphene Family Nanomaterial Reinforced Magnesium-Based Matrix Composites for Biomedical Application: A Comprehensive Review. *Metals* **2020**, *10*, 1002. [CrossRef]
4. Agnew, S.R.; Duygulu, Ö. Plastic Anisotropy and the Role of Non-Basal Slip in Magnesium Alloy AZ31B. *Int. J. Plast.* **2005**, *21*, 1161–1193. [CrossRef]
5. Wang, H.; Raeisinia, B.; Wu, P.D.; Agnew, S.R.; Tomé, C.N. Evaluation of Self-Consistent Polycrystal Plasticity Models for Magnesium Alloy AZ31B Sheet. *Int. J. Solids Struct.* **2010**, *47*, 2905–2917. [CrossRef]
6. Kurukuri, S.; Worswick, M.J.; Tari, D.G.; Mishra, R.K.; Carter, J.T. Rate Sensitivity and Tension-Compression Asymmetry in AZ31B Magnesium Alloy Sheet. *Philos. Trans. R. Soc. A Math. Phys. Eng. Sci.* **2014**, *372*, 20130216. [CrossRef]
7. Kurukuri, S.; Worswick, M.J.; Bardelcik, A.; Mishra, R.K.; Carter, J.T. Constitutive Behavior of Commercial Grade ZEK100 Magnesium Alloy Sheet over a Wide Range of Strain Rates. *Metall. Mater. Trans. A Phys. Metall. Mater. Sci.* **2014**, *45*, 3321–3337. [CrossRef]
8. Khan, A.S.; Pandey, A.; Gnäupel-Herold, T.; Mishra, R.K. Mechanical Response and Texture Evolution of AZ31 Alloy at Large Strains for Different Strain Rates and Temperatures. *Int. J. Plast.* **2011**, *27*, 688–706. [CrossRef]
9. Karimi, E.; Zarei-Hanzaki, A.; Pishbin, M.H.; Abedi, H.R.; Changizian, P. Instantaneous Strain Rate Sensitivity of Wrought AZ31 Magnesium Alloy. *Mater. Des.* **2013**, *49*, 173–180. [CrossRef]
10. Li, L.; Muránsky, O.; Flores-Johnson, E.A.; Kabra, S.; Shen, L.; Proust, G. Effects of Strain Rate on the Microstructure Evolution and Mechanical Response of Magnesium Alloy AZ31. *Mater. Sci. Eng. A* **2017**, *684*, 37–46. [CrossRef]
11. Korla, R.; Chokshi, A.H. Strain-Rate Sensitivity and Microstructural Evolution in a Mg-Al-Zn Alloy. *Scr. Mater.* **2010**, *63*, 913–916. [CrossRef]
12. Bhattacharya, B.; Niewczas, M. Work-Hardening Behaviour of Mg Single Crystals Oriented for Basal Slip. *Philos. Mag.* **2011**, *91*, 2227–2247. [CrossRef]
13. Nienaber, M.; Kurz, G.; Letzig, D.; Kainer, K.U.; Bohlen, J. Effect of Process Temperature on the Texture Evolution and Mechanical Properties of Rolled and Extruded AZ31 Flat Products. *Crystals* **2022**, *12*, 1307. [CrossRef]
14. Liu, B.; Yang, J.; Zhang, X.; Yang, Q.; Zhang, J.; Li, X. Development and Application of Magnesium Alloy Parts for Automotive OEMs: A Review. *J. Magnes. Alloy.* **2023**, *11*, 15–47. [CrossRef]
15. Hielscher, R.; Silbermann, C.B.; Schmidla, E.; Ihlemannb, J. Denoising of Crystal Orientation Maps. *J. Appl. Crystallogr.* **2019**, *52*, 984–996. [CrossRef]
16. Balint, D.S.; Deshpande, V.S.; Needleman, A.; Van Der Giessen, E. Size Effects in Uniaxial Deformation of Single and Polycrystals: A Discrete Dislocation Plasticity Analysis. *Model. Simul. Mater. Sci. Eng.* **2006**, *14*, 409–422. [CrossRef]
17. Ulacia, I.; Dudamell, N.V.; Gálvez, F.; Yi, S.; Pérez-Prado, M.T.; Hurtado, I. Mechanical Behavior and Microstructural Evolution of a Mg AZ31 Sheet at Dynamic Strain Rates. *Acta Mater.* **2010**, *58*, 2988–2998. [CrossRef]
18. Zheng, Z.; Balint, D.S.; Dunne, F.P.E. Rate Sensitivity in Discrete Dislocation Plasticity in Hexagonal Close-Packed Crystals. *Acta Mater.* **2016**, *107*, 17–26. [CrossRef]
19. Liu, J.; Fan, X.; Shi, Y.; Singh, D.J.; Zheng, W. The Effect of Strain Rate on the Deformation Processes of Nc Gold with Small Grain Size. *Crystals* **2020**, *10*, 858. [CrossRef]
20. Chapuis, A.; Liu, Q. Modeling Strain Rate Sensitivity and High Temperature Deformation of Mg-3Al-1Zn Alloy. *J. Magnes. Alloy.* **2019**, *7*, 433–443. [CrossRef]
21. Stohr, P.J.F.; Poirier, J.P. Etude En Microscopie Electronique Du Glissement Pyramidal (1122) (1123) Dans Le Magnesium. *Philos. Mag.* **1972**, *25*, 1313–1329. [CrossRef]
22. Reed-Hill, R.E.; Robertson, W.D. Deformation of Magnesium Single Crystals by Nonbasal Slip. *Jom* **1957**, *9*, 496–502. [CrossRef]
23. Obara, T.; Yoshinga, H.; Morozumi, S. {112−2}<1123> Slip System in Magnesium. *Acta Metall.* **1973**, *21*, 845–853. [CrossRef]
24. Wu, Z.; Ahmad, R.; Yin, B.; Sandlöbes, S.; Curtin, W.A. Mechanistic Origin and Prediction of Enhanced Ductility in Magnesium Alloys. *Science* **2018**, *359*, 447–452. [CrossRef] [PubMed]

Disclaimer/Publisher's Note: The statements, opinions and data contained in all publications are solely those of the individual author(s) and contributor(s) and not of MDPI and/or the editor(s). MDPI and/or the editor(s) disclaim responsibility for any injury to people or property resulting from any ideas, methods, instructions or products referred to in the content.